A Procedure for Correcting Radiosonde Reports for Radiation Errors

LARRY MCMILLIN AND MICHAEL UDDSTROM*

National Oceanic and Atmospheric Administration, National Environmental Satellite, Data, and Information Service, Satellite Research Laboratory, Washington, D.C.

ALESSANDRO COLETTI†

S M System and Research Corporation, Landover, Maryland

(Manuscript received 17 August 1991, in final form 18 March 1992)

ABSTRACT

Temperature sensors on radiosondes measure a temperature that is a balance between the temperature of the air and the temperature of the radiation environment of the sensor. Because of this balance, the temperature reported by a radiosonde differs from the true air temperature by an amount that is determined by the heat-transfer coefficient, the longwave emissivity of the sensor, the shortwave emissivity, the longwave flux on the sensor surface, the shortwave flux on the sensor surface, and the sensor temperature. Of these quantities, the heat-transfer coefficient is determined by properties of both the sensor and the atmosphere, the reflectivities are determined by the sensor, and the fluxes and air temperature are determined by the atmosphere. For a typical radiosonde, the radiative properties of the sensor can be determined, the coefficient of heat transfer can be estimated, and models exist for calculating the shortwave flux. In this paper, the authors show that a modification of the Elsasser formulation for infrared fluxes can be used to calculate the infrared flux. This provides sufficient information to solve for the temperature difference between the temperature sensor and the air. The method is used to calculate errors for some typical meteorological conditions for the white-coated VIZ sensor, made by VIZ Manufacturing Co.

The method was used to examine the range of radiation errors for typical conditions. Although the shortwave radiation error is generally recognized because it is observed in the day-to-night differences, it is demonstrated that the longwave radiation errors are significant and variable. The longwave error for the VIZ instrument can reach 3 K at 10 hPa for a winter profile and can exceed that when there is a stratospheric warming. While the longwave radiation error is generally considered to be a cooling effect, at 100 hPa the longwave radiation is a source of heating in a tropical atmosphere because the tropopause at 100 hPa is cold relative to the rest of the atmosphere that is radiating to the sensor. Clouds have significant effects on both the longwave and shortwave components. A cloud at the tropopause of a tropical atmosphere can change the error of a radiosonde above the cloud from a heating error to a cooling error. At sunrise and sunset, the change in the shortwave error is abrupt. Extremely accurate knowledge of the time and location of the radiosonde is required to reduce the uncertainty in temperature to less than 1 K at the upper levels at these times.

1. Introduction

The effect of radiation on the radiosonde temperature sensor has been known for some time. McInturff et al. (1979) used day–night differences to derive corrections for different radiosonde types. While this correction was a major improvement at the time it was implemented, it only accounts for some of the error sources. For example, at levels where there is a true diurnal cycle due to absorption of the shortwave radiation by ozone, the method does not separate the error from the true variation. In addition, radiosondes differ in their response to longwave radiation, and while the method described by McInturff et al. (1979) removes the diurnal component of the signal, radiosondes of different types can still be biased with respect to each other due to the longwave component. This problem is being addressed through the WMO (World Meteorological Organization) International Radiosonde Comparison (Nash and Schmidlin 1987). Ney et al. (1961) did an extensive analysis of the radiation errors for different types of sensors. They pointed out that making the sensor smaller, increasing the infrared reflectivity while keeping the visible reflectivity small, and changing the shape from a rod to a sphere all decrease the sensitivity of the sensor to the infrared environment. Talbot (1972) estimated typical radiation errors for the Australian radiosonde sensor that, at that time, used the same sensor that is used on the VIZ

* On leave from: New Zealand Meteorological Service, Wellington, New Zealand.

† Present affiliation: Italian Trade Commission—High Technology Center, New York, NY 10022.

Corresponding author address: Dr. Larry M. McMillin, R/RA14, Physics Branch, Satellite Research Laboratory NOAA/NESDIS, Washington, D.C. 20233.

instrument. The need for an improved operational correction was, however, demonstrated by McMillin et al. (1988). In that study, satellite measurements were used as a transfer standard to compare measurements from the VIZ and Vaisala RS80 instruments that are flown as part of the conventional radiosonde network. They found that the difference between the two types varies with the temperature profile. Luers (1990a,b) investigated the sensitivity of the VIZ sensor to various environmental effects. That study confirmed the conclusion of McMillin et al. (1988). Specifically, it was determined that the type of atmosphere and the amount of clouds are major influences on the radiation error experienced by the sensor. While that study provides some valuable insight into the errors caused by radiation effects and other environmental influences, it differs from our paper in that it was not designed to provide operational corrections for the effects and does not fulfill our need for a method to remove these errors from the radiosondes that are used to adjust coefficients for satellite retrievals.

2. The heat-transfer relationship

The relationship between the temperature of the air T_a and the temperature of the sensor T_s is given by

$$HA(T_s - T_a) = \epsilon R + \alpha S - \epsilon A \sigma T_s^4, \qquad (1)$$

where H is the convective heat-transfer coefficient, ϵ is the longwave emissivity of the sensor, α is the shortwave emissivity of the sensor, R is the total incoming longwave flux across the surface of the sensor, S is the total incoming shortwave flux across the surface of the sensor, A is the total surface area of the sensor, and σ is the Stefan–Boltzmann constant. Equation (1) can be easily solved for either T_a or the temperature error, which is simply the difference between T_s and T_a. The problem is determining the values of the other terms in the equation.

Some of the terms have been measured directly. For example, Schmidlin et al. (1986) give 0.86 as the value for ϵ and 0.12 as the value for α. The value of H depends on factors such as the velocity of the radiosonde and the density of the air. Williams and Acheson (1976) show that it is related to the time constant of the sensor through the relationship

$$H = \frac{m_t c}{\lambda A}, \qquad (2)$$

where m_t is the mass of the sensor, c its specific heat, and λ its time constant. The time constants for many radiosonde temperature sensors have been extensively studied and reported in the literature. They are, however, of limited value for this study because values of m_t and c, which can be easily determined by simple measurements, are not reported. Now that there is a method to correct radiosonde data that depends on knowing these parameters, it would be useful if values of m_t and c could be determined and made available. Since values of these parameters are not available, we use a more direct approach. Williams and Acheson (1976) give the convective heat-transfer coefficient as

$$H = \left(\frac{kC_1}{D}\right)\left(\frac{\rho v D}{\mu}\right)^m, \qquad (3)$$

where k is the thermal conductivity, D is the diameter of the sensor, v is the airspeed relative to the sensor, μ is the absolute viscosity of air, and values of C_1 and m are determined by the Reynolds number. We use the values given in their Table 1. For our purposes, the Reynolds number is between 1 and 4000, in which case they give

$C_1 = 0.891$, $m = 0.330$

for Reynolds numbers between 1 and 4;

$C_1 = 0.821$, $m = 0.385$

for Reynolds numbers between 4 and 40; and

$C_1 = 0.615$, $m = 0.466$

for Reynolds numbers between 40 and 4000.

We also use 0.12 g as the mass of the VIZ sensor, an estimate (the exact composition of the sensor is not available) that the specific heat capacity is 0.59 J g^{-1}, a length of 40 mm, a diameter of 1.27 mm, an assumed vertical velocity of the sensor relative to the air of 5 m s^{-1}, and an absolute viscosity μ of 0.000171 g (mm s^{-1}). We compute the Reynolds number from the relationship

$$\mathrm{Re} = (\rho v D/\mu), \qquad (4)$$

TABLE 1. Flux emissivities (%) for a plate for H_2O.

log$u$	−70°C	−40°C	−10°C	20°C
−5.0	2.16	1.90	1.86	1.96
−4.7	3.16	2.72	2.58	2.62
−4.3	5.11	4.40	4.11	4.09
−4.0	7.16	6.16	5.72	5.65
−3.7	9.78	8.41	7.81	7.68
−3.3	14.10	12.20	11.40	11.20
−3.0	18.00	15.70	14.60	14.30
−2.7	22.30	19.60	18.30	18.00
−2.3	28.30	25.10	23.6	23.20
−2.0	32.60	29.20	27.70	27.30
−1.7	36.80	33.30	31.90	31.60
−1.3	42.20	38.80	37.40	37.30
−1.0	46.20	42.80	41.70	41.80
−0.7	50.00	47.10	46.20	46.50
−0.3	56.00	53.50	52.90	53.60
0.0	61.10	59.10	59.00	60.00
0.3	67.30	66.20	66.60	67.70
0.7	77.40	77.80	78.80	79.80
1.0	85.30	86.80	88.10	88.80
1.3	91.50	93.80	95.10	95.40
1.7	95.80	98.00	98.80	98.70

and the thermal conductivity k [W m^{-2} (K m^{-1})$^{-1}$] from the relationship

$$k = \frac{2.64638 \times 10^{-3} T^{3/2}}{T_a + 245.4 \times 10^{-12/T_a}} \quad (5)$$

(*U.S. Standard Atmosphere, 1976*). With Eqs. (4) and (5), we have sufficient information to solve Eq. (3) for the value of the convective heat-transfer coefficient.

3. The shortwave effect

We also need to know the power being transferred to the sensor by incoming shortwave radiation. In a clear sky, the shortwave radiation striking a cylindrical sensor whose long axis is perpendicular to the azimuth angle to the sun is given by the intensity of the radiation times the cross section of the cylinder. In practice, the azimuth angle to the sun has an arbitrary angle relative to the axis of the cylinder, and this angle changes as the sensor rotates. Since this angle is not known at any given instant, it is common practice to assume the sensor rotates rapidly, and to calculate a response that is averaged over all angles. With these assumptions we need to average the angle of incidence on the cylinder over the azimuth angle. To do this, we need to know the angle at which a ray of light from the sun strikes the sensor. We are interested in the angle (Fig. 1) that, in the plane that is defined by the ray and the axis of the cylinder, is the angle between the ray and the cylinder axis. We define this angle as

$$\gamma = \cos^{-1}[\sin(\theta)\sin(\phi)], \quad (6)$$

where θ is the solar zenith angle and ϕ is the angle between the axis of the cylinder and the solar azimuth. When the solar energy is averaged over all azimuth angles, a weighting factor is determined that is 1.0 when the sun is overhead, but slightly less otherwise. The weighting factor is given by

$$E(m_a) = \frac{2}{\pi}\int_0^{\pi/2} (1 - \sin^2\theta \cos^2\phi)^{1/2} d\phi, \quad (7)$$

where $E(m_a)$ is the complete elliptic integral of the second kind and m_a is $\sin^2\theta$. Numerical approximations of this integral can be found in Abramowitz and Stegun (1964).

We must also account for the attenuation of solar radiation by the atmosphere. The intensity at the height of the radiosonde is given by

$$I = I_0 \exp[-\tau/\cos(\theta)], \quad (8)$$

where I_0 is the solar constant (1380 W m^{-2}) and τ is the optical thickness of the atmosphere. To calculate the average energy striking the sensor, I in Equation (8) is multiplied by the cross-sectional area of the cylinder times $E(m_a)$, giving

$$S = IAE(m_a). \quad (9)$$

Values of the optical thickness for various latitudes and seasons are given by McClatchey et al. (1971). Since the variations are small, we averaged McClatchey's results over all seasons and latitudes to obtain a single profile. A term could also be included for atmospheric scattering onto the sensor. Scattering from the surface and clouds are significant effects that are included. Finally, we include a correction for refraction at low solar elevation angles by using the Chapman function (Wilkes 1954). This allows sunlight to strike the sensor even when the sun is below the horizon.

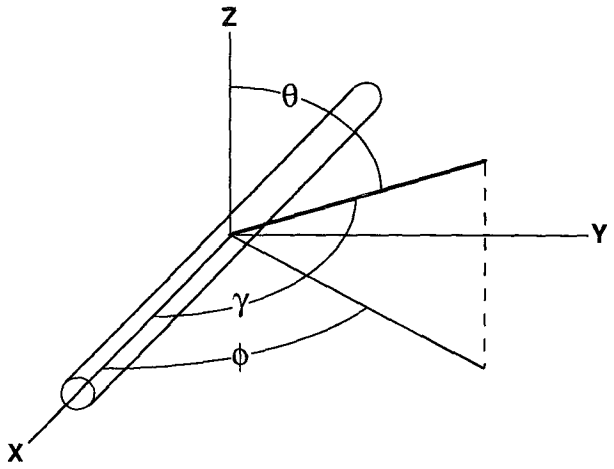

FIG. 1. Relationship of the angle γ between the sensor and a ray of light, with the solar zenith angle θ, and with the solar azimuth angle ϕ.

4. The longwave effect

The longwave radiation striking the sensor is modeled. Many methods exist for calculating the radiation along a path because of the importance of these calculations for remote sensing. Equivalent models are, however, difficult to find for flux calculations, which require an integration over many paths. In fact, the basic method of McMillin et al. (1979) could be easily adapted to flux calculations if the effective transmittances were available as a function of pressure for a diverse set of atmospheres. Unfortunately, existing algorithms for calculating fluxes provide the flux striking a flat plate, but cannot be easily modified to provide the effective transmittances that would be required to generate coefficients for a rapid transmittance method (McMillin et al. 1979). Certainly, this approach should be tried if the required transmittances become available. In this case extreme accuracy is not required because the flux calculation is needed to correct a radiosonde error of the order of several degrees. Thus, a flux calculation that is only 90% accurate will reduce the radiosonde uncertainty from several degrees to several tenths of a degree. Although the Elsasser method (Staley and Jurica 1970) is not as accurate as some

newer approaches, it is easy to use, well documented, and accurate enough for this application. For these reasons, the Elsasser formulation was selected. Even though the limitations of the Elsasser formulation are recognized, it is adequate for this use.

Although the Elsasser formulation can be used as a model, it needs to be modified for our use. In fact, it could be directly applied to a horizontally mounted flat plate, but radiosondes use thermistors in the shape of rods and beads, and the integration over all incoming angles leads to different results. To integrate over all the angles of the incoming radiation for the rod-shaped VIZ sensor, we use the result from the solar correction [Eq. (7)]. For the infrared, we treat θ in (7) as the angle of one beam of infrared radiation rather than the angle to the sun. We then calculate the weight for a given angle as

$$W(\theta) = E(1 - \sin^2\theta)2\Pi \sin\theta, \qquad (10)$$

and use the weight to calculate an average transmittance as

$$\tau_{\text{avg}} = \frac{\int_0^{\pi/2} W(\theta) \exp(-u \sec\theta) d\theta}{\int_0^{\pi/2} W(\theta) d\theta}, \qquad (11)$$

where u is the optical depth. Values of u are determined from flux emissivities given in percent by Staley and Jurica (1970) by first dividing by 100 and subtracting from 1.0 to obtain transmittances, then numerically solving for u given the transmittance. The numerical solution is performed using the polynomial approximations for the exponential integral of the first kind and a recurrence relation to obtain the value of the exponential integral of the second kind as explained in Abramowitz and Stegun (1964). The argument that provides the given value of the transmittance is the value of u that is used in (10) to produce an average transmittance for the cylinder. This average transmittance is then converted to a flux emissivity by subtracting the value from 1.0 and multiplying by 100. The original flux emissivities given by Staley and Jurica (1970) and the revised flux emissivities, which are valid for cylindrical surface, are given in Tables 1 and 2 for water vapor, Tables 3 and 4 for carbon dioxide, and Tables 5 and 6 for ozone. The revised values are appropriate for a horizontal cylinder. It should be noted that, while Tables 5 and 6 are given for completeness when satellite data are used to extend the profile above the last level reported by the radiosonde, they were not used for the results shown in this paper. Instructions for using the tables to calculate fluxes are given in Staley and Jurica (1970). We include clouds by placing the appropriate values of emissivity and reflectivity at the given level. In the case of radiation reflected from either clouds or the surface, we calculate the atmospheric transmittance for the total path from an emitting layer to the reflecting level, then to the sensor.

TABLE 2. Flux emissivities (%) for a cylinder for H_2O.

log$u$	−70°C	−40°C	−10°C	20°C
−5.0	2.29	2.01	1.97	2.07
−4.7	3.35	2.88	2.73	2.78
−4.3	5.42	4.66	4.36	4.34
−4.0	7.59	6.53	6.06	5.99
−3.7	10.36	8.91	8.28	8.14
−3.3	14.91	12.91	12.07	11.86
−3.0	19.01	16.60	15.44	15.12
−2.7	23.52	20.69	19.33	19.01
−2.3	29.79	26.45	24.88	24.46
−2.0	34.26	30.72	29.16	28.74
−1.7	38.61	34.98	33.53	33.22
−1.3	44.17	40.67	39.23	39.12
−1.0	48.28	44.79	43.66	43.76
−0.7	52.16	49.20	48.28	48.59
−0.3	58.25	55.72	55.11	55.82
0.0	63.38	61.38	61.27	62.28
0.3	69.57	68.48	68.87	69.96
0.7	79.47	79.85	80.82	81.78
1.0	87.01	88.41	89.62	90.27
1.3	92.74	94.80	95.95	96.21
1.7	96.56	98.43	99.08	99.00

TABLE 3. Flux emissivities (%) for a plate for CO_2.

log$h$	−70°C	−40°C	−10°C	20°C
−4.0	0.11	0.12	0.12	0.11
−3.7	0.16	0.17	0.17	0.16
−3.3	0.25	0.26	0.26	0.25
−3.0	0.33	0.35	0.35	0.34
−2.7	0.44	0.47	0.47	0.45
−2.3	0.64	0.69	0.69	0.67
−2.0	0.86	0.93	0.93	0.91
−1.7	1.19	1.29	1.30	1.27
−1.3	1.92	2.08	2.11	2.07
−1.0	2.78	3.03	3.08	3.03
−0.7	3.92	4.30	4.39	4.32
−0.3	5.76	6.36	6.54	6.49
0.0	7.19	7.99	8.26	8.23
0.3	8.60	9.61	10.00	10.00
0.7	10.40	11.70	12.30	12.40
1.0	11.70	13.30	13.90	24.10
1.3	13.00	14.80	15.60	15.80
1.7	14.70	16.70	17.70	18.00
2.0	15.90	18.10	19.30	19.60
2.3	17.00	19.50	20.70	21.10
2.7	18.60	21.30	22.70	23.10
3.0	19.70	22.60	24.10	24.40
3.3	20.70	23.90	25.40	25.70

5. Sensitivity studies

The model was used to generate radiosonde errors for some typical conditions to evaluate the importance of some of the meteorological variables. We used two profiles for our sensitivity studies. One profile, flight TC2012, was flown at San Juan, Puerto Rico, at 1507 UTC 6 June 1987. It is one of the special three sensor

TABLE 4. Flux emissivities (%) for a cylinder for CO_2.

log$h$	−70°C	−40°C	−10°C	20°C
−4.0	0.118	0.128	0.128	0.118
−3.7	0.168	0.178	0.178	0.168
−3.3	0.259	0.270	0.270	0.259
−3.0	0.343	0.363	0.363	0.353
−2.7	0.458	0.490	0.490	0.469
−2.3	0.670	0.723	0.723	0.702
−2.0	0.904	0.978	0.978	0.957
−1.7	1.25	1.36	1.37	1.34
−1.3	2.03	2.20	2.23	2.19
−1.0	2.95	3.21	3.26	3.21
−0.7	4.16	4.56	4.65	4.58
−0.3	6.11	6.74	6.93	6.88
0.0	7.62	8.47	8.75	8.72
0.3	9.11	10.18	10.59	10.59
0.7	11.01	12.38	13.02	13.12
1.0	12.38	14.07	14.70	14.91
1.3	13.75	15.65	16.49	16.70
1.7	15.54	17.65	18.70	19.01
2.0	16.81	19.12	20.38	20.69
2.3	17.96	20.59	21.84	22.26
2.7	19.64	22.47	23.94	24.36
3.0	20.80	23.83	25.40	25.72
3.3	21.84	25.19	26.76	27.07

flights flown by Schmidlin (Schmidlin et al. 1986), and was selected because it is typical of tropical conditions. The temperature and humidity profiles for this sounding are shown in Fig. 2. A second profile, flight TC1885, taken at Bismark, North Dakota, at 1704 UTC 8 February 1989 was selected for contrast to the tropical profile. Profiles of temperature and water vapor for this flight are shown in Fig. 3. For radiation errors, the important differences are the difference in water vapor at the surface, the difference between the tropical and winter tropopause structures, the difference in stratospheric temperatures, and the difference in surface albedo.

TABLE 5. Flux emissitivies (%) for a plate for O_3.

logh_{O_3}	−70°C	−40°C	−10°C	20°C
−4.0	0.109	0.155	0.191	0.214
−3.7	0.167	0.239	0.300	0.340
−3.3	0.284	0.412	0.520	0.594
−3.0	0.415	0.610	0.777	0.896
−2.7	0.588	0.872	1.12	1.29
−2.3	0.900	1.34	1.72	1.99
−2.0	1.20	1.79	2.30	2.68
−1.7	1.53	2.31	2.99	3.51
−1.3	1.99	3.03	3.97	4.71
−1.0	2.30	3.54	4.66	5.55
−0.7	2.59	4.01	5.30	6.33
−0.3	2.97	4.60	6.10	7.29
0.0	3.24	5.02	6.64	7.93
0.3	3.47	5.36	7.08	8.43
0.7	3.71	5.68	7.47	8.84
1.0	3.83	5.84	7.65	9.03

TABLE 6. Flux emissivities (%) for a cylinder for O_3.

logh_{O_3}	−70°C	−40°C	−10°C	20°C
−4.0	0.117	0.163	0.199	0.223
−3.7	0.175	0.248	0.311	0.353
−3.3	0.295	0.428	0.543	0.621
−3.0	0.432	0.638	0.816	0.942
−2.7	0.615	0.917	1.18	1.36
−2.3	0.946	1.41	1.82	2.11
−2.0	1.27	1.89	2.44	2.84
−1.7	1.62	2.45	3.17	3.72
−1.3	2.11	3.21	4.21	4.99
−1.0	2.44	3.75	4.94	5.88
−0.7	2.74	4.25	5.62	6.71
−0.3	3.15	4.88	6.47	7.73
0.0	3.43	5.32	7.04	8.40
0.3	3.68	5.68	7.50	8.93
0.7	3.93	6.02	7.92	9.36
1.0	4.06	6.19	8.11	9.57

The model requires information that is not contained in a radiosonde report. It needs to know the solar zenith angle, the temperature of the earth's surface, the visible and infrared emissivities of the earth's surface, the cloud amount and cloud emissivity, and the brightness temperature of the radiation from the atmosphere that is above the top of the radiosonde report. Estimates of these quantities exist at major forecast centers. Values that we used for these parameters are contained in the figure legends.

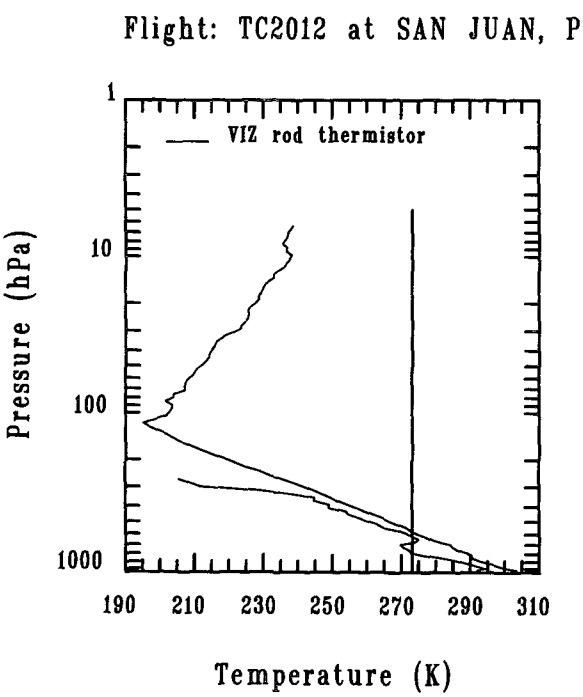

FIG. 2. Temperature and humidity profiles for flight TC2012, a tropical profile from a radiosonde launched at 1507 UTC 6 June 1987 at San Juan, Puerto Rico.

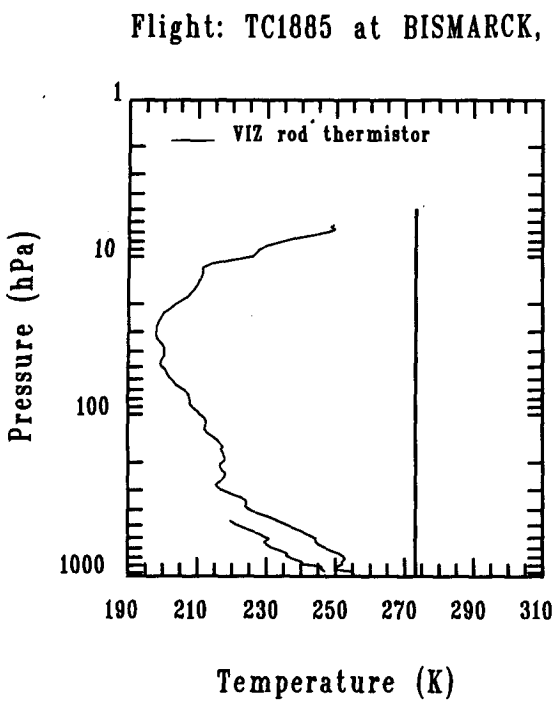

FIG. 3. Temperature and humidity profiles for flight TC1885, a winter profile from a radiosonde launched at 1704 UTC 8 February 1989 at Bismark, North Dakota.

Figure 4 shows the sensitivity to the surface skin temperature. Using flight TC1885, the winter case, the skin temperature was set to three values corresponding to differences from the surface air temperature of −20, 0, and +20 K. The curves show that most of the difference in radiation was absorbed in the first level of the atmosphere. Above the surface layer, a 20-K change in surface temperature produces a temperature change of about 0.1 K. This increases to about 0.4 K at 10 hPa because the air is less dense. Thus, at high altitudes, a given difference in the radiation-energy balance requires a bigger change in temperature between the atmosphere and the sensor to balance the total energy than at low altitudes. This effect is observed even though the difference in the radiation energy balance is reduced with height by the intervening atmosphere. It should be noted that this atmosphere is fairly dry with the result that the errors are near the maximum values that would be observed. When the same parameters were used for flight TC2012, the tropical case, the additional moisture increased the atmospheric absorption to the extent that the curves for the three temperatures converged to a single line between 900 and 100 hPa, and had a maximum spread of less than 0.1 K at 10 hPa.

Figure 5 demonstrates the sensitivity to solar zenith angle. Errors for flight TC2012, the tropical case, are shown at solar zenith angles of 0°, 30°, 60°, 90°, and 120°. As might be expected, the biggest change (about 1.2 K at 10 hPa) occurs between 120°, which is dark, and 90°, where light is already striking the sensor because of refraction and because the radiosonde is above the earth's surface. Relatively little (<0.2 K) change occurs near the local zenith, as shown by the difference in error between 0° and 30°.

Figures 6–10 demonstrate the sensitivity to clouds. Figure 6 shows errors at night for flight TC1885, the polar case, for clouds located at 850, 500, 300, and 100 hPa. The clear value is shown as a reference. When the radiosonde is below the cloud, the radiation from the cloud is greater than the radiation from cold space and the sensor becomes slightly warmer than it would be without the cloud. The effect is largest for the higher clouds because a sensor near the earth's surface receives most of its incoming energy from the warm atmosphere near the sensor and little from cold space. When the radiosonde passes through the clouds, the clouds block the warm radiation from the surface, and the radiosonde experiences a cooling effect. For a cloud at 100 hPa, the change in error is about 0.5 K as the radiosonde passes through the cloud. The magnitude of these effects is profile dependent. Figure 7 shows the effects of the same parameters on flight TC2012, the tropical case. For this atmosphere, the effects are enhanced, resulting in a change of 1.7 K for a cloud at 100 hPa.

In daylight, the differences are reduced. When the sensor is above the cloud, the decrease in infrared flux

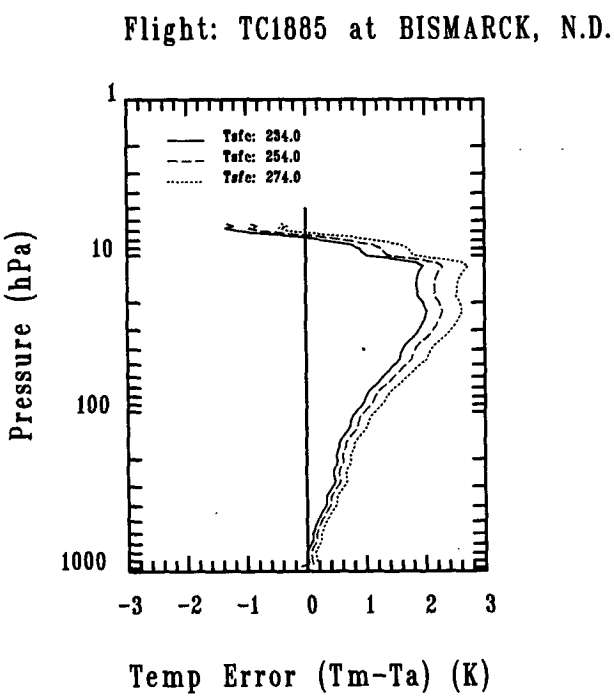

FIG. 4. Radiosonde errors for three different surface temperatures for profile TC1885. No clouds were present, the visible emissivity of the surface was 0.2, the solar zenith was 60°, and the radiating temperature of the atmosphere above the radiosonde was 150 K.

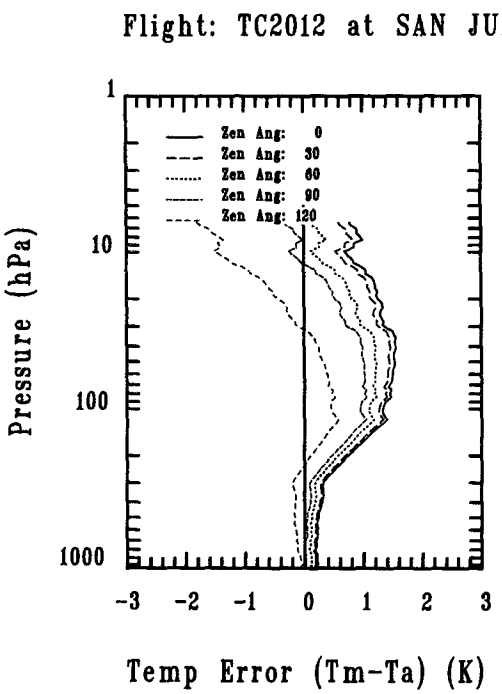

FIG. 5. Radiosonde errors for five different solar zenith angles for profile TC2012. The surface temperature was equal to the temperature at 1000 hPa, the surface emissivity for visible radiation was 0.2, no clouds were present, and the radiating temperature of the atmosphere above the radiosonde was 150 K.

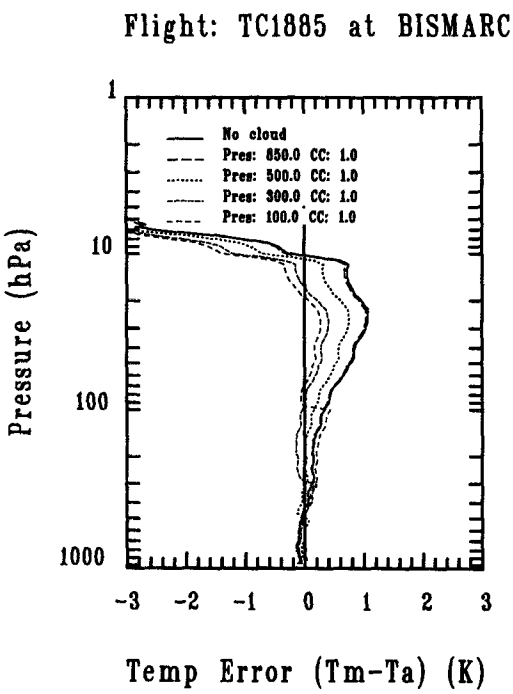

FIG. 6. Radiosonde errors for a clear sky and for four different cloud heights for profile TC1885 at night. The conditions are the same as those in Fig. 4 except that the solar zenith angle was 60°, and 100% cloud cover with an emissivity of 0.8 was assumed.

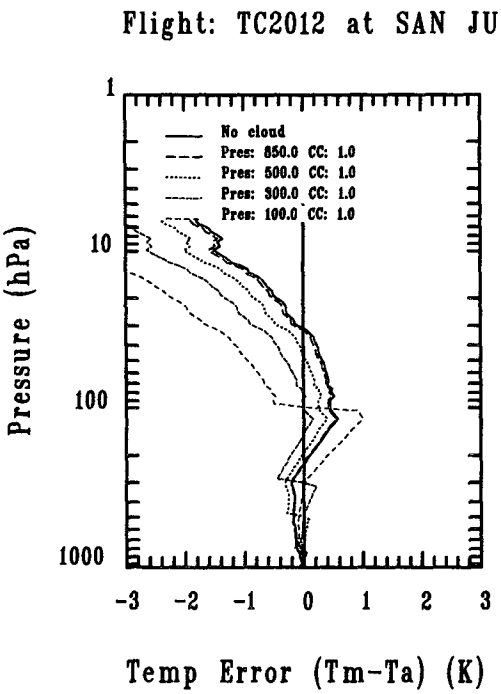

FIG. 7. Radiosonde errors for a clear sky and for four different cloud heights for profile TC2012 for the conditions listed in Fig. 6.

from the ground is accompanied by an increase in solar radiation reflected from the clouds. Daylight conditions for the two flights shown in Figs. 6 and 7 are shown in Figs. 8 and 9. It should be noted that the sudden increase and decrease that occurs at the cloud pressure is artificial. It occurs because the cloud is placed at a single level, allowing the warm radiation from below and the increased solar radiation to occur at the same level. If the cloud were modeled as a layer, the warm radiation from the surface would be absorbed before the increased solar radiation became effective. Thus, the current calculations are valid for all levels above and below the modeled cloud level, but should not be used at the actual level of the cloud in daylight conditions. With this caveat, it can be seen that, with the conditions modeled in Fig. 8, the cooling effect above the clouds that was seen in Fig. 6 has been replaced by a warming for clouds at 850 hPa due to the increased solar radiation. Figure 9 shows the cases modeled in Fig. 7 under daylight conditions. In this case, the clouds still cause a cooling as the radiosonde passes through the cloud level, but the magnitude is reduced by the reflected solar radiation. Again, clouds near the surface (850 and 500 hPa) cause a net warming, while higher clouds cause a cooling. In Fig. 8, a surface albedo typical of bare ground was used. Since Bismark is often snow covered in winter, the conditions used in Fig. 8 were modeled again with the surface albedo set to 0.6, a value that is typical of a surface covered by snow. Results for these conditions are shown in Fig. 10. In these

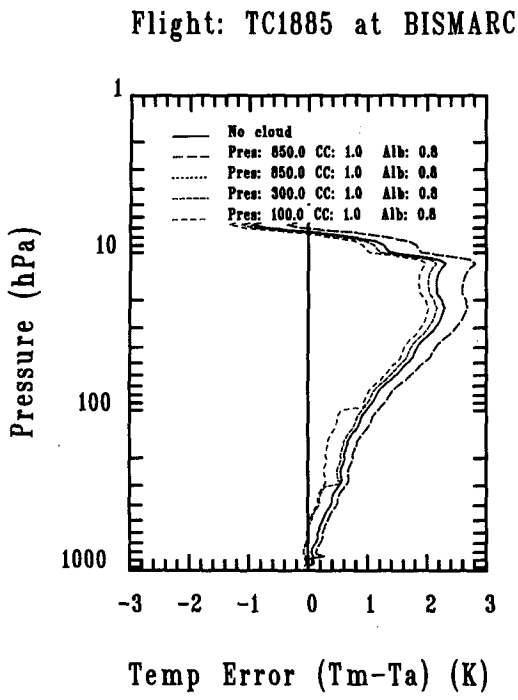

FIG. 8. Radiosonde errors for a clear sky and for four different cloud heights for profile TC1885 in daylight.

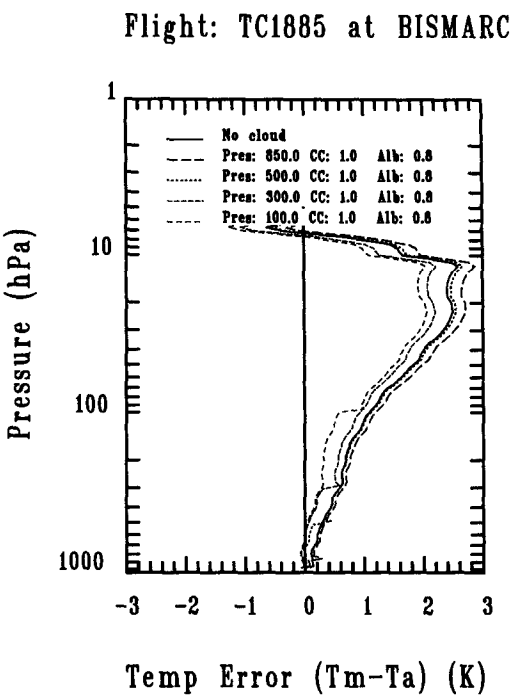

FIG. 10. Radiosonde errors for a clear sky and for four different cloud heights for profile TC1885 for the conditions shown in Fig. 8 except the surface albedo has been set to 0.6, the appropriate value for snow.

conditions, the radiosonde is warmer under the cloud due to the additional solar radiation reflected from the surface. Under clear skies, the difference between snow and bare ground exceeds 0.5 K at 100 hPa, and 1.0 K at 10 hPa. The lesson to be learned from all these figures is that the effect of clouds is highly variable and strongly dependent on conditions such as the type of atmosphere, the solar zenith angle, the surface albedo, and the emissivities of the sensor. While the cloud effects on the VIZ sensor tend to cancel in daylight, there is still a significant difference between the error caused by a cloud at 100 hPa and one at 850 hPa. Cloud effects are also significant when there is extensive high-level cloud in a tropical sounding at night. A model that includes these effects should make a more accurate correction than one that considers only the change in solar elevation angle.

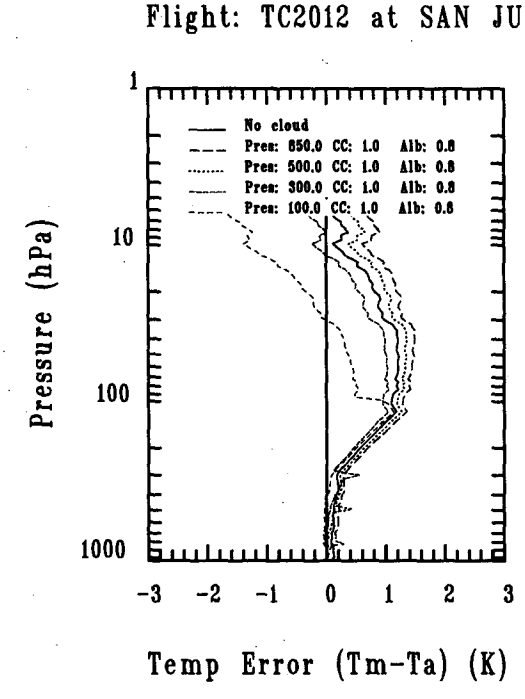

FIG. 9. Radiosonde errors for a clear sky and for four different cloud heights for profile TC2012 for the conditions shown in Fig. 8.

As mentioned previously, for these flights it was necessary to assign values to some parameters that would be measured by satellites and readily available at a major forecast center. One of these quantities is the radiance emitted by the atmosphere above the highest level reported by the radiosonde. We generated this quantity by supplying a "lid" temperature. Since satellite measurements will be available when the model is used, the dependence of the correction on this temperature is not an overriding issue. Nevertheless, it seemed prudent to examine this effect. Figure 11 shows the effect of different lid temperatures on flight TC1885, the winter flight. Since flux is a nonlinear function of temperature, the largest effect occurs for the warmest

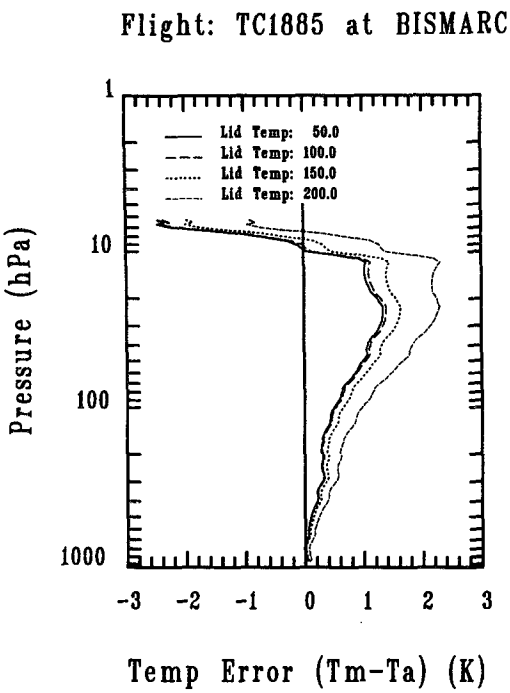

FIG. 11. Radiosonde errors for different lid temperatures for flight TC1885 for the conditions listed in Fig. 4. The surface skin temperature was set equal to the surface air temperature.

temperatures. At 100 hPa, a change in the lid temperature from 150 to 200 K causes a change in sensor temperature of 0.7 K. The error due to a change from 100 to 150 K is barely significant. Similar effects are observed for flight TC2012 that are not shown. The largest lid temperatures are, however, observed in the stratospheric warmings that are associated with profiles like flight TC1885. This means that even though the sensitivities of the two atmospheres are similar, the variation in lid temperature (and thus the effect) is much smaller in the tropics.

Figure 12 demonstrates the effect of different atmospheres on the radiation error. It shows the error for nighttime conditions for the two atmospheres: TC2012 and TC1885. The difference is large, particularly in the upper regions. The difference is small at the surface as expected; it increases to 0.4 K at 300 hPa, crosses zero at 200 hPa, increases to 0.4 K at 100 hPa, crosses zero again at 70 hPa, grows to 2.0 K at 12 hPa, then crosses zero again between 7 and 8 hPa. It should be noted that the features shown are profile dependent. The two profiles, however, show features that are characteristic of their type. For example, a sensor in a tropical profile experiences infrared heating near the tropopause where the sensor is cold relative to the atmospheric layers above and below the sensor. In contrast, a sensor in a polar sounding experiences infrared heating at a higher level, and then cooling. This is the result of a mild warming of the upper atmosphere. Near 10 hPa, the sensor is relatively cold, yet is receiving energy from the warmer atmosphere above. When the sensor enters the warmer layers, it becomes warm, thus greatly increasing its outgoing radiation and causing the sensor to become cold relative to the warm air to maintain the energy balance. It should be noted that the stratospheric temperatures observed in flight TC1885 are cold compared to those observed in some stratospheric warming events. This figure illustrates the dependence of the radiation correction on the profile shape that was noted by McMillin et al. (1988).

6. Some practical considerations

Our correction procedure was developed to provide corrections for the operational radiosondes used to evaluate and tune satellite retrievals. Since we plan to use the method to correct radiosondes for satellite matches, estimates of surface skin temperature, the upper-atmospheric temperature and ozone profiles, and the cloud parameters will be available. The split-window observations (McMillin and Crosby 1984) from the satellite will provide the skin temperature, the cloud parameters retrieved from the satellite will provide an estimate of average cloud conditions (Nappi et al. 1988) that can be combined with the estimates made from the radiosonde profile, and the temperatures of the layers above the end of the radiosonde report can be provided by satellite data. A major me-

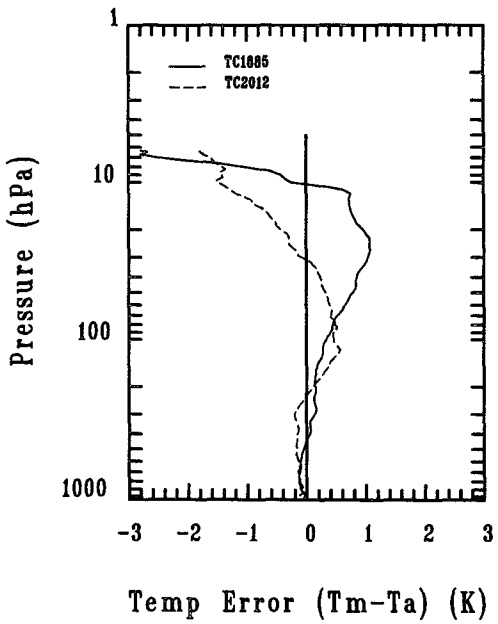

FIG. 12. Radiosonde errors at night for two different profiles. The conditions were the same as those in Fig. 4 except the solar zenith angle was fixed at 120° to simulate nighttime.

teorological center will also have reliable estimates of these values based on a combination of satellite observations, analysis, forecasts, or all three. For these and other reasons, we recommend that this procedure be applied at a center where these data are available, rather than at the radiosonde stations. If any corrections are made at the stations, they must be made in such a way that the original observations can be recovered. For radiosondes without corresponding satellite information, these quantities can be estimated. The alternatives are to provide no correction or to provide an average correction. Incorporating more physics by producing actual corrections for the variables that can be estimated, and using average conditions only for the unknown variables, has to be better than applying no correction or applying one based only on average values of all components.

Another alternative would be to provide sensors that are less sensitive to radiation effects. For example, a thin platinum wire should increase the sensitivity to the temperature at the radiosonde pressure relative to the rest of the atmosphere, but that approach would increase the cost of the instruments. There may be cheaper alternatives that can produce the same effect. It is difficult to assess this possibility, because few measurements of emissivities of possible coatings are available, some materials degrade with age, and many of the ones in the literature represent laboratory values that are not representative of values that could be achieved in the field. Alternative coatings should be investigated since discovery of a cheap coating with the appropriate properties could essentially eliminate the longwave radiation errors without increasing the shortwave errors. In this regard, we strongly support the recommendations of Ney et al. (1961). Emissivities should be as small as possible in both wavelength regions.

7. Summary and conclusions

We have developed a model for calculating radiation errors for radiosonde sensors given their radiative properties. Using this model we have examined the sensitivity of radiosondes to various factors. For the VIZ rod thermistor, used extensively in the United States until recently, and still used in the eastern part of the country, we find the following effects:

- The surface skin temperature has a relatively small effect on radiosonde error because, once the radiosonde leaves the boundary layer, most of the surface radiation is absorbed before it reaches the sensor.
- Because the atmosphere is relatively transparent to solar radiation, high surface albedos and clouds increase the reflected solar radiation and have a relatively large effect on the radiosonde error. In the case of clouds, the increased solar radiation tends to be compensated by a decrease in the infrared radiation from the surface, minimizing the total error in daylight.
- The solar zenith angle has a significant effect on the radiation error. The largest effect occurs as the sensor passes from darkness into daylight. The sensitivity becomes less near the zenith. But it must be recognized that this effect is a function of sensor shape since most of the change results from the change in the exposure of the horizontal rod to the sun's rays. Above the horizon, the dependence on the solar zenith angle would be greatly reduced for a spherical sensor. Since the exact time, location, and elevation of radiosondes as functions of pressure are not known, there will always be a large uncertainty about the radiation effects for radiosondes that are launched near the earth's terminator. Errors for radiosondes launched at other longitudes can be modeled more accurately.
- The atmosphere has a significant effect on the radiation error. Since the radiation emitted by the radiosonde is a large component of the energy balance, radiosondes in a warm environment radiate more than those in a cold environment, and this effect changes more than the incoming radiation. A radiosonde near a clear tropical tropopause will actually be heated by the radiation from the warm surface and the warm layers near the surface, while a radiosonde above a cloud at the tropopause will experience increased cooling because the warm radiation will be blocked.

It is interesting to note that the temperature of the sensor is the most important factor in the infrared energy balance. This occurs because the sensor radiates energy at a rate that is proportional to the temperature of the sensor raised to the fourth power, while changes in the incoming flux tend to be small. The latter occurs because the incoming flux is determined by the average temperature of a thick layer of the atmosphere. An atmosphere that is warm at some level tends to be cold at another level to keep the total mass constant. This is illustrated by a tropical atmosphere that is warmer than a polar atmosphere at the surface, but colder at the tropopause. The resulting difference in flux striking the sensor is small because the large flux from the lower levels of a tropical atmosphere is offset by a small flux from the tropopause region. Thus, a radiosonde sensor in a relatively warm region of an atmosphere radiates more energy than it does in a colder region, but the incoming fluxes tend to be the same. The difference in energy balance must be made up by a change in the transfer of energy with the surrounding air. In a stratospheric warming event, the radiosonde in the upper atmosphere becomes very warm with relatively little change in the incoming flux. In these conditions, a radiosonde sensor experiences enhanced cooling. While the atmospheric effect is most evident in the long wavelength region, a clear, dry polar atmosphere also has significantly less solar absorption than a hazy, wet tropical one. The model should be modified to include

some atmospheric dependence of the visible attenuation.

As a result of this study, it is our conclusion that the infrared effects can be significant if they are ignored or treated as a single average. At the same time, we have demonstrated that we can model these effects quite well using the information available from the radiosonde, and even better if coincident satellite sounding is available. On the other hand, the solar radiation is largely determined by clouds and surface conditions that are not as well known for a specific flight. Therefore, given a choice of radiosonde coatings, we recommend optimizing the solar reflectivity to minimize the uncertainties, and modeling the infrared effects. Of course, every effort should be made to reduce emissivities in both regions. With this approach, errors in the VIZ-type radiosonde can be reduced from the order of several degrees to tenths of a degree.

Acknowledgments. The work of M. J. Uddstrom was supported under the Resident Research Associateship of the National Research Council of the National Academy of Sciences.

REFERENCES

Abramowitz, M., and I. A. Stegun, 1964: Handbook of Mathematical Functions with Formulas, Graphs, and Mathematical Tables. National Bureau of Standards Applied Mathematics Series 55, 1046 pp. [Available from the Superintendent of Documents, U.S. Government Printing Office, Washington, D.C. 20402.]

Luers, J. K., 1990a: The influence of environmental factors on the temperature of the radiosonde thermistor. Ph.D. thesis, University of Tennessee. [Available from University Microfilms International, A Bell & Howell Information Company, 300 N. Zeeb Road, Ann Arbor, MI 48106.]

——, 1990b: Estimating the temperature error of the radiosonde rod thermister under different environments. *J. Atmos. Oceanic Technol.*, **7,** 882–895.

McClatchey, R. A., R. W. Fenn, J. E. Selby, F. E. Voltz, and J. S. Garing, 1971: Optical Properties of the Atmosphere, (rev.), Air Force Cambridge Research Laboratories, AD A726116.

McInturff, R. M., F. G. Finger, K. W. Johnson, and J. D. Laver, 1979: Day–night differences in radiosonde observations of the stratosphere and troposphere. NOAA Tech. Memo. NWS NMC 63, 47 pp.

McMillin, L. M., and D. S. Crosby, 1984: Theory and validation of the multiple window sea surface temperature technique. *J. Geophys. Res.*, **89,** 3655–3661.

——, H. E. Fleming, and M. L. Hill, 1979: Atmospheric transmittance of an absorbing gas. 3: A computationally fast and accurate transmittance model for absorbing gases with variable mixing ratios. *Appl. Opt.*, **18,** 1600–1606.

——, M. E. Gelman, A. Sanyal, and M. Sylva, 1988: A method for the use of satellite retrievals as a transfer standard to determine systematic radiosonde errors. *Mon. Wea. Rev.*, **116,** 1091–1102.

Nash, J., and F. J. Schmidlin, 1987: WMO International Radiosonde Comparison (U.K. 1984, U.S.A. 1985). Instruments and Observing Methods Rep. No. 30, WMO/TD-No. 195, 111 pp.

Nappi, A. J., A. Swaroop, and L. M. McMillin, 1988: An improved method for the retrieval of cloud height and amount from satellite radiance measurements. Preprints, *Third Conference on Satellite Meteorology and Oceanography,* Anaheim, Calif., Amer. Meteor. Soc., 388–391.

Ney, E. P., R. W. Maas, and W. F. Huch, 1961: The measurement of atmospheric temperature. *J. Meteor.*, **18,** 60–80.

Schmidlin, F. J., J. K. Luers, and P. D. Huffman, 1986: Preliminary estimates of radiosonde thermistor errors. NASA Tech. Paper 2637, 15 pp.

Staley, D. O., and G. M. Jurica, 1970: Flux emissivity tables for water vapor, carbon dioxide, and ozone. *J. Appl. Meteor.*, **9,** 365–372.

Talbot, J. E., 1972: Radiation influences on a white-coated thermistor temperature sensor in a radiosonde. *Aust. Meteor. Mag.*, **20,** 22–33.

U.S. Standard Atmosphere, 1976: NOAA-S/T76-1562, 227 pp.

Wilkes, M. V., 1954: A table of Chapman's grazing incidence integral $\mathrm{ch}(x, \chi)$, *Proc. Phys. Soc.*, **b.67,** 304–308.

Williams, S. L., and D. T. Acheson, 1976: Thermal time constants of U.S. radiosonde sensors used in GATE. NOAA Tech Mem. EDS CEDDA-7, 16 pp.